Imaging human epithelial properties with polarized light-scattering spectroscopy

RAJAN S. GURJAR[1], VADIM BACKMAN[2], LEV T. PERELMAN[1], IRENE GEORGAKOUDI[1], KAMRAN BADIZADEGAN[3], IRVING ITZKAN[1], RAMACHANDRA R. DASARI[1] & MICHAEL S. FELD[1]

[1]*G.R. Harrison Spectroscopy Laboratory, Massachusetts Institute of Technology, Cambridge, Massachusetts, USA*

[2]*Biomedical Engineering Department, Northwestern University, Evanston, Illinois, USA*

[3]*Department of Pathology, Children's Hospital, Harvard Medical School, Boston, Massachusetts, USA*

Correspondence should be addressed to V.B.; email: v-backman@northwestern.edu

Biomedical imaging with light-scattering spectroscopy (LSS) is a novel optical technology developed to probe the structure of living epithelial cells *in situ* without need for tissue removal. LSS makes it possible to distinguish between single backscattering from epithelial-cell nuclei and multiply scattered light. The spectrum of the single backscattering component is further analyzed to provide quantitative information about the epithelial-cell nuclei such as nuclear size, degree of pleomorphism, degree of hyperchromasia and amount of chromatin. LSS imaging allows mapping these histological properties over wide areas of epithelial lining. Because nuclear enlargement, pleomorphism and hyperchromasia are principal features of nuclear atypia associated with precancerous and cancerous changes in virtually all epithelia, LSS imaging can be used to detect precancerous lesions in optically accessible organs.

Light scattering spectroscopy (LSS) is extensively used in physical sciences to study a great variety of systems. Biological tissue can also be studied with LSS. It has been demonstrated that light scattering can provide structural and functional information about the tissue[1,2]. One important biomedical application of optical imaging and spectroscopy is non-invasive or minimally invasive detection of pre-cancerous and early cancerous changes in human epithelium, such as dysplasia or carcinoma *in situ*. Detection of such conditions is particularly important because 85% of all cancers originate in the epithelium, and most such lesions are readily treated if diagnosed at an early stage. However, many forms of precancerous changes are difficult to detect and diagnose using conventional techniques, which require histological examination of biopsies obtained from visible lesions or random surveillance biopsies. Changes in the nuclei of the epithelial cells are amongst the most important indicators for dysplasia[3,4]. The major diagnostic criteria include nuclear enlargement, increased variation in nuclear size and shape (pleomorphism), and increased concentration of chromatin, leading to darker staining of the nuclear material (hyperchromasia). LSS can provide quantitative, objective measurements of these parameters in real time without the need for tissue removal. Until now, this technique has been restricted to sampling of millimeter-size regions of tissue using a contact probe[5]. Here we present an LSS-based imaging technique which can map variations in the size of epithelial-cell nuclei of living tissues over wide surface areas. The resulting images provide direct quantitative measures of nuclear enlargement and chromatin content, which can be translated into clinical diagnoses. The technique can be used for non-invasive or minimally invasive detection of precancerous changes in a variety of organs, such as the colon and oral cavity.

Light-scattering spectroscopy

The angular and wavelength distributions of the light scattered by a cell nucleus depend on nuclear size and refractive index. Thus, if light directly backscattered from the nuclei is observed, the size and refractive index of these nuclei can be obtained from the spectral variations of the signal[2,6]. However, these single-scattering events are masked in biological tissue. The light scattered back from a tissue specimen can be divided into two parts: one due to single-scattering events, and the background due to multiply scattered light (diffusive background). To study the single-scattering component, one needs first to distinguish it from the diffusive background. Polarized incident light can be used to accomplish this. The principles of this technique have been described[7] and applied to study oral epithelium morphology[8]. The method is based on the fact that linearly polarized light incident on a turbid medium such as biological tissue loses its polarization as it traverses the medium. A small portion of the incident light is backscattered by the epithelial cells, retaining its polarization in this single-scattering event. The remainder diffuses into the underlying tissue and is depolarized by multiple scattering. Thus, by removing the unpolarized component of light emerging from the tissue, the contribution due to the backscattering from epithelial cells can be readily distinguished. The resulting spectrum can then be analyzed to extract the size distribution of the nuclei, their population density and their refractive index relative to that of the cytoplasm[7]. The nuclear refractive index is higher due to the presence of chromatin, and so the chromatin content can be obtained from the refractive index. As discussed below, the resolution provided by LSS exceeds the pixel size of an imaging CCD and the wavelength of light used to measure the sizes of cell nuclei, in contrast to conventional optical techniques. It has been shown that polarization could be used to differentiate underlying structure in human skin imaging[9–11]. Others have imaged the spatial distribution of polarized light multiply scattered from cell suspensions[12,13]. However, none of these studies attempted to extract morphological features of the scatterers.

Ex vivo tissue studies

We performed experiments on three types of systems: Physical tissue models consisting of an optically thin layer of polystyrene beads imbedded in gelatin on top of a diffusive substrate; monolayers of T84 tumor colon cells; and *ex vivo* tissues. Studies with physical models and cell monolayers were used to calibrate the experimental setup and to estimate measurement accuracy. We found the size measurements to be ac-

		Morphometry		LSS	
Normal mucosa	Mean nuclear diameter and standard error of measurement, μm	5.60	0.20	5.70	0.13
	Standard deviation of nuclear diameters, μm	1.01		0.82	
Adenoma	Mean nuclear diameter and standard error of measurement, μm	7.44	0.23	7.67	0.40
	Standard deviation of nuclear diameters, μm	1.59		2.19	

Table 1 Comparison of the values of the mean nuclear diameters and standard deviations of nuclear sizes in the colon adenoma of Fig. 2*a* and surrounding non-dysplastic epithelium measured with LSS and using standard morphometry of the stained tissues.

curate to 0.025 μm, and the refractive index measurements to be accurate to 0.001. This illustrates that LSS imaging can elucidate subtle morphological variations such as a difference in nuclear size of a fraction of a micron.

The *ex vivo* colon tissue samples were obtained immediately after resection from patients undergoing colectomy for familial adenomatous polyposis. Colonic adenomas are precancerous dysplastic lesions. Typical adenomas are polypoid structures that can vary in size from less than a millimeter to several centimeters, and are covered by an epithelial layer exhibiting all of the characteristics of dysplastic lesions, including cell nuclear enlargement, pleomorphism and hyperchromasia. The adenomas are surrounded by normal tissue covered by a single layer of epithelial cells. We imaged an adenoma surrounded by non-dysplastic colon mucosa using the LSS apparatus (Fig. 1). As outlined in Methods, a series of polarized images at different wavelengths were taken, and the spectra were analyzed for each pixel of the imaged field. The parameters obtained were the size and refractive index of the nuclei in each pixel. The imaged field was 1.3×1.3 cm. Fig. 2*a* shows a 2×2-mm region of resected colon tissue with the adenoma, about 1 mm in diameter, in the center. The field was divided in smaller regions of 125×125 μm, and the percentage of nuclei larger than 10 μm was obtained for each of these areas. Our previous studies have shown that this statistic, which characterizes the degree of nuclear enlargement, is highly significant for diagnosis of dysplastic lesions in the colon and several other organs[5,14].

The resulting color-coded plot is shown in Fig. 3*a*. As expected, the nuclei are enlarged in the central, adenomatous region, but not in the surrounding tissue. To verify these results, after the LSS measurements we studied stained tissue sections of both the polyp and surrounding normal region. Fig. 2*c* shows a histological section of the same polyp. The size of each stained nucleus was measured, and the average size of the dysplastic nuclei was estimated. A similar procedure was carried out for a normal region surrounding the polyp. Table 1 lists the resulting average sizes and standard deviations for both the polyp and normal regions, obtained from the LSS measurements, along with the corresponding values obtained by standard morphometry. The average size of the nuclei in the normal region is smaller than those in the polyp, with a smaller standard deviation. Fig. 3*b* is a map of the spatial distribution of the mass of nuclear solids (DNA, RNA, proteins and so forth), displayed in units of picograms per nucleus. These values were derived from the knowledge of the diameter and the refractive index of the nuclei, obtained from our LSS image. The nuclear solid mass correlates with the chromatin content. In the region of the polyp, the chromatin content is larger than in the surrounding normal tissue. This condition is an indication of dysplasia. The resulting values are in good agreement with the results reported elsewhere[15–18].

As further proof of LSS imaging ability, Fig. 2*b* shows a colonic polyp from another patient who underwent partial colectomy for adenocarcinoma arising in the setting of a polyposis syndrome. The LSS image of the polyp and the surrounding region was obtained. Although the clinical presentation was suggestive of an adenoma, Fig. 3*c* and *d* show that the spatial distribution of nuclear size is uniform, with very few enlarged or hyperchromatic nuclei. Histological examination of the polyp (Fig. 2*d*) by an expert pathologist verified our findings and showed a benign polyp with no dysplasia. Furthermore, histological examination of all polyps from this patient was diagnostic for juvenile polyposis syndrome with no dysplasia. This illustrates that LSS imaging can differentiate dysplastic from non-dysplastic polyps, even when the macroscopic appearance of the lesions is so similar that an experienced clinician could not differentiate the two.

Discussion

We have developed a new biomedical imaging modality based on polarized LSS, which is capable of providing morphological information about epithelial cells *in situ*. In contrast to conventional images of cells or tissues, the LSS-based imaging provides quantitative images of the histological properties, such as nuclear enlargement, pleomorphism and increased chromatin content. Methods for providing such quantitative information without tissue removal are not currently available. It is important to emphasize that, in contrast to conventional optical images, the images produced by LSS do not depict tissue structure as a microphotograph would. Rather, they provide quantitative maps of the spatial distributions of parameters such as nuclear

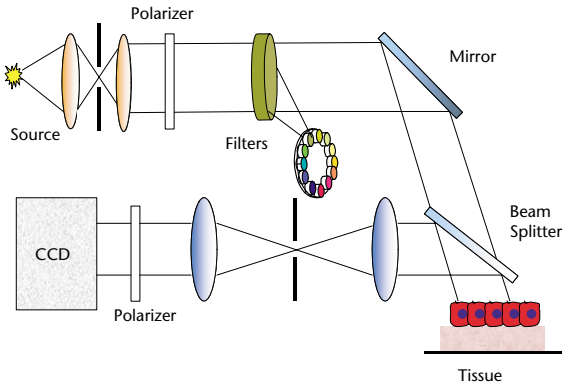

Fig. 1 Schematic diagram of the polarized LSS imaging apparatus. The light delivery train consists of an arc lamp source, collimating achromatic lens, broadband polarizer, one of the narrowband wavelength-selecting filters, beam splitter and mirror. The light collection train consists of relay lens system, angle-selecting aperture, rotating analyzing polarizer and CCD. The distances between the first of the two lenses of the relay system and the tissue sample, between the lenses and the aperture, and between the second lens and the CCD are all equal to the focal distance of these lenses. Thus, the spatial distribution of light emerging from the tissue surface in a solid angle selected by the aperture is imaged onto the CCD.

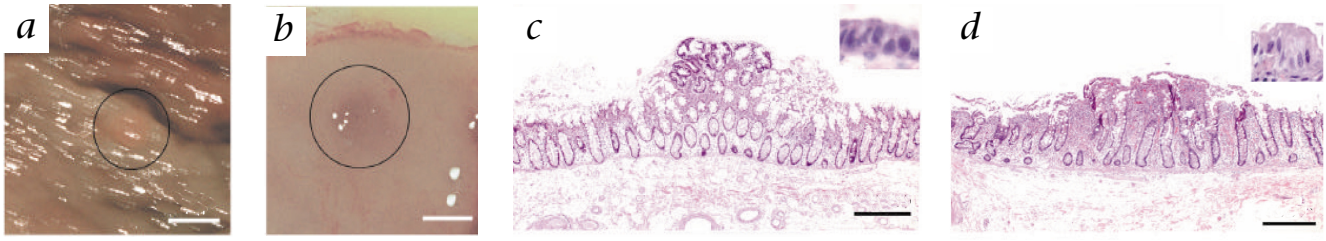

Fig. 2 Gross and microscopic photographs of colonic polyps used for LSS imaging shown in Fig. 3. ***a*** and ***b***, Two polyps highlighted by circles. Although the polyps are grossly similar, only one of them is dysplastic. Histological features identify polyp (*a*) as an adenoma and polyp (*b*) as an inflammatory polyp with no dysplasia. Scale bars, 1 mm. ***c*** and ***d***, Microscopic sections of these polyps. Insets show each polyp's surface epithelium at high magnification, illustrating dysplastic nuclear features in *c* but not in *d*. Representative photomicrographs from each polyp and the surrounding normal tissue were used to measure the average diameter of the nuclei and their variations in size. Scale bars, 0.5 mm.

Methods

LSS imaging device. Fig. 1 shows the set-up for LSS-based imaging. A 75 W xenon arc lamp (Oriel Instruments, Stratford, Connecticut) illuminates the sample that can be living tissue, a cell monolayer or a physical tissue model. The light from the lamp is collimated, polarized and transmitted through one of 11 narrowband (4-nm) filters (Edmund Scientific, Tonawanda, New York) to select the desired wavelength, λ_i i = 1–11, in the range 450–700 nm. This beam is delivered to the sample surface and illuminates an area of ~5 cm^2. A pair of equifocal achromatic lenses separated by twice their focal length collects the light backscattered from the sample. An aperture positioned at the center of the lens system ensures that the CCD detector (Princeton Instruments, Trenton, New Jersey), placed one focal length away from the outer lens, collects only light scattered in a solid angle corresponding to a half angle of 0.5°. Such a small angle of collection ensures that the major contribution to the signal is due to light scattered by the largest structures inside the cells, cell nuclei[2,7,8]. This scheme allows 1:1 imaging of the illuminated surface. The CCD detector consists of an array of 512 × 512 pixels, with each pixel having dimensions 25 × 25 μm. The analyzer is rotated to select the polarization state of the backscattered light. The CCD collects 2 images for each of the 11 illumination wavelengths. The first image, $I_{\parallel}(\lambda_i;x,y)$, with (x,y) pixel coordinates and wavelength λ, is taken with the analyzer oriented to collect backscattered light that is polarized along the polarization direction of the incident light. The second image, $I_{\perp}(\lambda_i;x,y)$, is taken with the analyzer oriented to collect the orthogonally polarized component. We then subtract $I_{\perp}(\lambda_i;x,y)$ from $I_{\parallel}(\lambda_i;x,y)$ to remove the contribution from unpolarized diffusive background. This procedure results in an image $\Delta I(\lambda_i;x,y) = I_{\parallel}(\lambda_i;x,y) - I_{\perp}(\lambda_i;x,y)$ constituted almost entirely from single-scattered photons, which, for most epithelial tissues, corresponds to a sampling depth of 30–50 μm (ref. 7). To compensate for the cross-talk between neighboring pixels, we constructed new images for each wavelength, in which the intensity of any pixel is a weighted average of the values $\Delta I(\lambda_i;x,y)$ of the adjacent pixels from the original image[19].

Calibration of the LSS imaging device. We performed experiments with physical models and cell monolayers to calibrate the experimental set-up and estimate measurement accuracy. The experiments with physical models employed an optically thin layer of polystyrene beads (optical thickness τ = 0.3) of several diameters, d = 4.5, 6 and 10 μm, with standard deviation of diameters $\sigma \approx 0.03$ μm, suspended in polyethylene glycol. The relative refractive index of the beads in glycol, 1.066, is in the range of relative refractive indices of biologically relevant structures, which typically vary between 1.02 and 1.10. The experiments with cell monolayers used two-layered media to model living tissue. The upper layer, a monolayer of T84 colon tumor cells grown on a glass slide, simulated epithelium. The lower layer, an optically thick gel containing a mixture of powdered Ba_2SO_4 to provide scattering and human blood to provide absorption, simulated underlying connective tissue. In each case 11 images $\Delta I(\lambda_i;x,y)$ were obtained for each of the wavelengths λ_i. The resulting spectra were in good agreement with the backscattered signals predicted by Mie theory[20].

Analysis of LSS signals. The spectra collected with the LSS imaging device were analyzed using the Mie theory-based inversion procedure reported in ref. 7. We have already established that the Mie theory of light scattering by spherical particles of arbitrary size enables prediction of the major spectral variations of light scattered by cell nuclei. In our studies, the scatterers were assumed to be normally distributed in size. Mie theory was used to generate a database of LSS spectra over a range of mean diameters (from 0.1 μm to 20 μm in 0.005-μm steps), standard deviations (from 0.1 μm to 5 μm in 0.005-μm steps), and average relative refractive indexes (from 1.02 to 1.1 in 0.0005 steps). The sizes and refractive indexes of the scatterers that best fit the data were found. The wide range of sizes incorporated in the database ensured that the non-nuclear contribution to LSS signals was not ignored. Experiments with polystyrene beads of known size enabled us to estimate the accuracy of this inversion procedure. We found the size measurements to be accurate to 0.025 μm, and the refractive index measurements to be accurate to 0.001.

***Ex vivo* tissue studies.** *Ex vivo* tissue studies were performed on discarded portions of freshly resected specimens maintained in HBSS. The measurements took about 10 min. The imaged regions were marked, and all tissue specimens were submitted to pathology for microscopic examination. Estimation of nuclear solid mass was based on previous studies that have established that refractive index of nuclei and many other cell organelles is a linear function of the ratio of solid mass of an organelle and its volume. LSS allows direct measurement of the refractive index and size of a nucleus. To estimate nuclear volume from a known size, the nuclei were assumed to be spherical, which is a reasonable approximation considering their random orientation in tissues with respect to the direction of light propagation. Therefore, the nuclear solid mass can be evaluated from known nuclear refractive index and volume, which are directly measured with LSS (refs. 7,15–18).

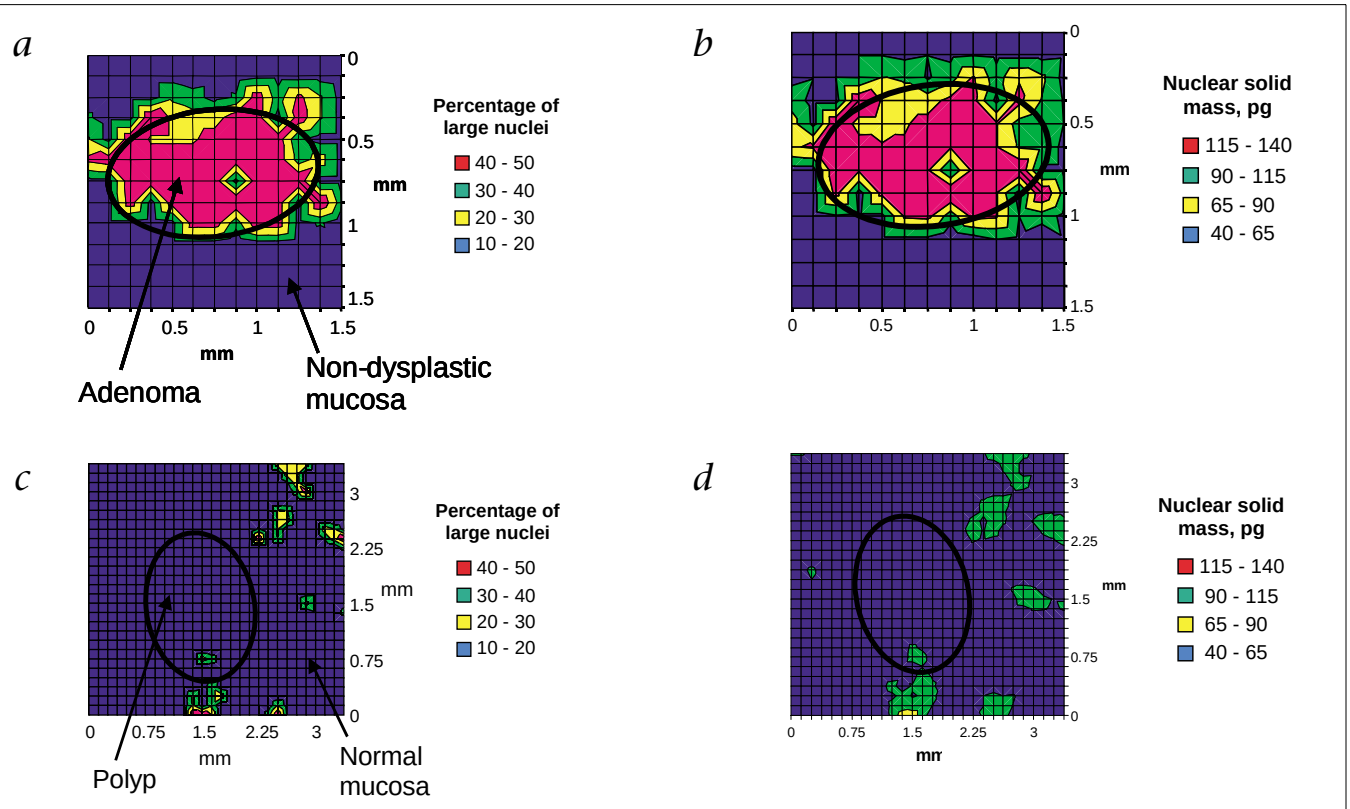

Fig. 3 LSS images of colon tissue samples. ***a*** and ***b***, LSS images showing the spatial distribution of the percentage of enlarged nuclei and nuclear solid mass for the polyp of Fig. 2*a*, respectively; ***c*** and ***d***, LSS images showing the spatial distribution of the percentage of enlarged nuclei and nuclear solid mass for the polyp of Fig. 2*b*, respectively. The polyps are marked by ellipses in *c* and *d*.

enlargement, degree of pleomorphism, and increased chromatin content—features that relate to the functional state of the tissue. Furthermore, pixel size and the wavelength of light do not limit the resolution of the technique. For example, in our tissue images, the nuclear size is determined with an accuracy exceeding 0.1 μm, whereas the pixel size is 25 μm and the light wavelength approximately 0.5 μm. Such accuracy is obtainable because the information is derived from spectral variations of the backscattered light—an interference phenomenon sensitive to very small changes in the cell nuclear parameters. LSS makes it possible to observe these variations, and measuring them enables the nuclear size and refractive index to be determined. The results reported here indicate the promise of LSS-based imaging for clinical use, and as a biomedical research tool to study the dynamics of nuclear changes accompanying the progression of cancer and other diseases. Particularly important applications include detection of early cancer and precancerous conditions in cervix and oral cavity.

Acknowledgments

We thank W. Lencer for T84 cells and S. Fulghum for useful comments. This study was supported by NIH grant P41-RR02594, NIH grant R01-CA53717 and CIMIT grant 731-3489-5.

1. Mourant, J.R. *et al.* Spectroscopic diagnosis of bladder cancer with elastic light scattering. *Laser Surg. Med.* **17**, 350–357 (1995).
2. Perelman, L.T. *et al.* Observation of periodic fine structure in reflectance from biological tissue: A new technique for measuring nuclear size distribution. *Phys. Rev. Lett.* **80**, 627–630 (1998).
3. Cotran, R.S., Robbins, S.L. & Kumar, V. *Robbins pathological basis of disease* (W.B. Saunders, Philadelphia, Pennsylvania, 1994).
4. Boone, C.W. *et al.* Quantitative grading of rat esophageal carcinogenesis using computer-assisted image tile analysis. *Cancer Epidemiol. Biomarkers Prevention* **9**, 495–500 (2000).
5. Backman, V. *et al.* Diagnosing cancers using spectroscopy. *Nature* **406**, 35–36 (2000).
6. Perelman, L.T. *et al.* Quantitative analysis of mucosal tissues in patients using light scattering spectroscopy. *Optical Tomography and Spectroscopy of Tissue III* (eds., Alfano, R.R., Chance, B. & Tromberg B.J.) 3597, 474–479 (SPIE Press, Bellingham, Washington, 1999).
7. Backman, V. *et al.* Polarized light scattering spectroscopy for quantitative measurement of epithelial structures *in situ*. *IEEE J. Sel. Topics Quantum Electron* **5**, 1019–1027 (1999).
8. Sokolov, K., Drezek, R., Gossage, K. & Richards-Kortum, R. Reflectance spectroscopy with polarized light: Is it sensitive to cellular and nuclear morphology? *Opt. Express* **5**, 302–317 (2000).
9. Anderson, R.R. Polarized light examination and photography of the skin. *Arch. Dermatol.* **127**, 1000–1005 (1991).
11. Jacques, S.L., Roman, J.R. & Lee, K. Imaging superficial tissues with polarized light. *Lasers Surg. Med.* **26**, 119–129 (2000).
12. Demos, S.J. & Alfano, R.R. Optical polarized imaging. *Appl. Opt.* **36**, 150–155 (1997).
13. Bartel, S. & Hielscher, A.H. Monte Carlo simulations of the diffuse backscattering Muller matrix for highly scattering media. *Appl. Opt.* **39**, 1580–1588 (2000).
14. Sankaran, V., Schonenberger, S., Walsh, J.T. Jr & Maitland, D.J. Polarization discrimination of coherently propagating light in turbid media. *Appl. Opt.* **38**, 4252–4261 (1999).
15. Wallace, M. *et al.* Endoscopic detection of dysplasia in patients with Barrett's esophagus using light scattering spectroscopy. *Gastroenterology* **119**, 677–682 (2000).
16. Davies, H.G. in *General Cytochemical Methods* Vol. I (ed., Danielli, J.F.) (Academic Press, New York and London, 1958).
17. Brown, G.L., McEwan, M. & Pratt, M. Macromolecular weight and size of deoxypentose nucleic acids. *Nature* **176**, 161–162 (1955).
18. Davies, H.G., Deeley, E. M. & Denby, E.F. Attempts at measurement of lipid, nucleic acid and protein content of cell nuclei by microscope-interferometry. *Exp. Cell Res.* Suppl. **4**, 136–149 (1957).
19. Lee, L., Pappelis, A.J., Pappelis, G.A. & Kaplan, H.M. Cellular and nuclear dry mass and area changes during human oral mucosa cell development. *Acta Cytol.* **17**, 214–219 (1973).
20. Russ, J.C. in *The Image Processing Handbook* (CRC Press, Boca Raton, Ann Arbor, London, Tokyo, 1992).
21. Van de Hulst, H.C. in *Light Scattering by Small Particles* (Dover, New York, 1957).